CONTRAST MEDIA & MOLECULAR IMAGING

Received: 14 May 2011, Revised: 23 July 2011, Accepted: 5 August 2011, Published online in Wiley Online Library: 2012

(wileyonlinelibrary.com) DOI: 10.1002/cmmi.479

Polyglycerol-grafted superparamagnetic iron oxide nanoparticles: highly efficient MRI contrast agent for liver and kidney imaging and potential scaffold for cellular and molecular imaging

Nasser Arsalani[a]*, Hassan Fattahi[a,b], Sophie Laurent[b], Carmen Burtea[b], Luce Vander Elst[b] and Robert N. Muller[b]*

Polyglycerol as a water-soluble and biocompatible hyperbranched polymer was covalently grafted on the surface of superparamagnetic iron oxide nanoparticles. With this aim, superparamagnetic magnetite nanoparticles were prepared by coprecipitation in aqueous media, then the surface of nanoparticles was modified to introduce the reactive groups on the surface of nanoparticles. After that, polyglycerol was grafted on the surface of nanoparticles by ring-opening anionic polymerization of glycidol using *n*-bulyllithium as initiator. The magnetometry, relaxometry and phantom MRI experiments of this highly stable ferrofluid showed its high potential as a negative MRI contrast agent. Calculated r_1 and r_2 relaxivities at different magnetic fields were higher than the values reported for commercially available iron oxide contrast agents. The *in vivo* MRI studies showed that, after intravenous injection into mice, the particles produced a strong negative contrast in liver and kidneys, which persisted for 80 min (in liver) to 110 min (in kidneys). The negative contrast of the liver and kidneys weakened over the time, suggesting that polyglycerol coating renders the nanoparticles stealth and possibly optimal for renal excretion. Copyright © 2012 John Wiley & Sons, Ltd.

Keywords: iron oxide nanoparticles; superparamagnetism; polyglycerol; MRI; molecular imaging; contrast agent; nanomedicine

1. INTRODUCTION

Since magnetic resonance imaging (MRI) provides noninvasive, three-dimensional examination of biological events in living organisms, it is one of the most powerful diagnostic tools in modern clinical medicine (1). The MRI mechanisms are based on excitation and relaxation of hydrogen nuclei that are abundant in water and lipids of tissue. Differences in intrinsic longitudinal (T_1) and transverse (T_2) relaxation times of different parts of the tissues induce changes of MR signal intensity, which in turn result in an imaging contrast. The relaxation times can be manipulated by the use of T_1 (e.g. gadolinium chelates) and T_2 (e.g. particulate iron oxide) contrast agents, producing brighter (T_1-weighted) and darker (T_2-weighted) images, where they are accumulated (2–4). However, gadolinium complex contrast agents are effective only when present in millimolar concentrations (5). Because of their superparamagnetic property, iron oxide nanoparticles have been found to be effective at lower concentrations and can better serve as contrast enhancement agents for MRI (6–10).

Apart from serving as contrast enhancement agents, superparamagnetic iron oxide nanoparticles have many other applications in nanomedicine and biomedical research, such as targeted drug delivery (11,12), tumor hyperthermia (13), biological separation (14) and biosensors (15). However, challenges in fabricating and processing nanoparticles for bioapplications include particle agglomeration and biocompatibility. These challenges become greater as nanoparticles are further scaled down in size. The high surface area-to-volume ratio of these nanoparticles results in a tendency to aggregate and interact with plasma proteins upon intravenous injection, leading to rapid clearance by the reticuloendothelial system (16,17). Thus, nanoparticles are commonly protected with a hydrophilic and biocompatible polymer coating to improve their dispersity and stability. Commonly investigated polymers for this purpose include dextran (18), poly(vinyl alcohol) (19), poly(D,L-lactide-co-glycolide) (20), poly(ethylene glycol) (21) and poly(vinyl pyrrolidone) (22,23).

* *Correspondence to: N. Arsalani, Polymer Research Laboratory, Department of Organic and Biochemistry, Faculty of Chemistry, University of Tabriz, 29 Bahman Blvd, Tabriz, Iran.*
E-mail: arsalani@tabrizu.ac.ir

R. N. Muller, Department of General, Organic and Biomedical Chemistry, NMR and Molecular Imaging Laboratory, University of Mons, Avenue Maistriau 19, B-7000, Mons, Belgium.
E-mail: robert.muller@umons.ac.be

a *N. Arsalani, H. Fattahi*
Polymer Research Laboratory, Department of Organic and Biochemistry, Faculty of Chemistry, University of Tabriz, 29 Bahman Blvd, Tabriz, Iran

b *H. Fattahi, S. Laurent, C. Burtea, L. V. Elst, R. N. Muller*
Department of General, Organic and Biomedical Chemistry, NMR and Molecular Imaging Laboratory, University of Mons, Avenue Maistriau 19, B-7000, Mons, Belgium

Depending on the type of interactions, two methods are used to modify the iron oxide nanoparticles by polymers. These methods are based on either physical interactions or chemical bonding and are 'noncovalent' and 'covalent' approaches, respectively. The noncovalent approach is based on Van der Waals interactions between nanoparticles and polymers and includes dispersion with the low molar mass polymers, polymer wrapping and polymer adsorption. In the covalent approach, molecules or macromolecules are grafted onto the surface of nanoparticles through chemical linkages. This method is very effective because grafted macromolecules have increased stability in physiological media (24–27).

Hyperbranched polyglycerol is water soluble and, taking the biocompatibility of polyether structures such as poly(ethylene glycol) into account, its polyether backbone makes it an attractive polymer for biomedical and pharmaceutical applications (28–30). This hyperbranched polymer bears hydroxyl groups on the periphery, allowing modification for end user purposes (31,32). Recently, Wang *et al*. have prepared polyglycerol-grafted magnetite nanoparticles and evaluated their efficiency as MRI contrast agents *in vitro* (33). They have immobilized a reactive hydroxyl group on the surface of magnetite nanoparticles via ligand exchange of oleic acid with 6-hydroxy caproic acid. In order to form macroinitiators on the surface, the hydroxyl groups were treated with aluminum isopropoxide and then glycidol was polymerized on the surface. The r_1 and r_2 relaxivities measured at 1.5 T were found to be 6.64 and 64.2 $mM^{-1}\,s^{-1}$, respectively, and the calculated r_2/r_1 ratio was 9.7. Polyglycerol-grafted nanoparticles had an M_s value of 30 emu g^{-1} and *in vitro* studies showed that the uptake of polyglycerol (PG)-grafted nanoparticles by macrophages was very low, even when cultured with a relatively high magnetic nanoparticles concentration. These results motivated us to prepare the PG-grafted magnetic nanoparticles in such a way that all the bonds were completely covalent without ligand exchange (since this phenomenon can also happen in physiological media, leading to nanoparticle agglomeration) and also to investigate their *in vivo* biodistribution in mice by MRI, followed by the measurement of blood plasma and urine concentration.

In the present study, superparamagnetic Fe_3O_4 nanoparticles were synthesized through coprecipitation method and modified subsequently with 3-aminopropyl triethoxysilane (APTES). Then hyperbranched PG was grafted on modified magnetite nanoparticles through the 'grafting from' method. Since the polyglycerol was bound to the surface of magnetite nanoparticles through covalent bonds, the prepared ferrofluid was very stable for a long period of time. T_2-Weighted MRI images of PG-grafted magnetic nanoparticles were obtained at different concentrations using 7 T MRI. *In vivo* MRI studies were performed in mice at different times after intravenous injection, to follow the biodistribution of the nanoparticles.

2. EXPERIMENTAL

2.1. Materials

Ferric chloride haxahydrate ($FeCl_3.6H_2O$, >99%), ferrous chloride tetrahydrate ($FeCl_2{\cdot}4H_2O$, >99%), ammonium hydroxide (25 wt%) and glycidol were purchased from Fluka. 3-Aminopropyltriethoxysilane, butyllithium (15% solution in *n*-hexane), and dichloromethane were obtained from Merck. All the materials mentioned above were used without further purification. Toluene and *n*-hexane were obtained from Merck (Germany) and were dried by refluxing over sodium prior to use. Ethanol (96%) was provided by Simin Tak (Qazvin, Iran). The dialysis bag (MWCO: 12000) was purchased from Sigma-Aldrich (Germany).

2.2. Synthesis of Fe_3O_4 nanoparticles

The preparation of Fe_3O_4 nanoparticles was performed by a chemical co-precipitation of Fe^{2+} and Fe^{3+} ions as described previously (34). Briefly, 50 ml of 1.0 mol l^{-1} Fe^{2+} and 2.0 mol l^{-1} Fe^{3+} solutions were prepared with deionized water in two beakers, and then transferred to a 250 ml three-necked flask together. The solution was heated to 80 °C, NH_4OH (25 wt%) was added dropwise under argon protection and vigorous mechanical stirring was applied to reach pH 10–11. The mixture was heated at 80 °C for 1 h, and then the precipitated powders were collected by magnetic separation. The obtained magnetic nanoparticles were washed with deionized water five times and then with ethanol three times, and were dried to powder at 40 °C under vacuum. Magnetic nanoparticles were obtained with a yield of 98.3%.

2.3. Preparation of APTES-modified Fe_3O_4 nanoparticles

The surface of Fe_3O_4 was coated with APTES by a silanization reaction to obtain modified magnetic nanoparticles (MNPs) with amine groups according to a previous report (35). Briefly, 4.225 g of MNPs were mixed with ethanol (100 ml) using ultrasound to produce a homogeneous suspension, to which 16.16 g of APTES was added under argon atmosphere. To obtain the optimal surface modification, the molar ratio of APTES to Fe_3O_4 was applied as 4:1 (36). The reaction mixture was kept at room temperature for 5 h under a nitrogen atmosphere with vigorous mechanical stirring. Then the obtained APTES-immobilized MNPs were washed with ethanol (2×30 ml) and dichloromethane (2×30 ml) in turn. Finally, APTES-modified nanoparticles were dried under vacuum at 40 °C.

2.4. Synthesis of polyglycerol-grafted Fe_3O_4 nanoparticles

Polyglycerol-grafted Fe_3O_4 nanoparticles were prepared through surface-initiated polymerization of glycidol in a reactor equipped with a mechanical stirrer under an argon atmosphere. APTES-modified nanoparticles (0.5 g) were deprotonated with 0.375 ml butyllithium (15% solution in *n*-hexane) for 2 h at room temperature. The butyllithium solution was removed via a syringe and nanoparticles were washed with dried *n*-hexane several times under argon atmosphere. Then 50 ml of dried toluene was added to the flask, and nanoparticles were dispersed ultrasonically in toluene for 1 h under argon protection. A mixture of glycidol (2 ml) and toluene (10 ml) was slowly added at 95 °C over 6 h. After a further 24 h, the product was separated magnetically and washed with diethylether and then dried. For further purification, the product was dispersed in distilled water and dialyzed for 4 days by changing the external water every 8 h.

2.5. Characterization techniques

2.5.1. Fourier transform infrared spectroscopy

Fe_3O_4, APTES-modified Fe_3O_4 and PG-grafted Fe_3O_4 nanoparticles were tested by Fourier transform infrared (FT-IR) spectroscopy. The measurements were performed on a Tensor 27

spectrometer (Bruker, Germany) with a solid potassium bromide method, using 2 cm^{-1} resolution and 10 scanning times.

2.5.2. *Transmission electron microscopy*

The size and shape of nanoparticles were observed with transmission electron microscope (TEM; Joel TEM-2100, Japan) operated at 200 kV. For TEM investigation, the nanoparticles were deposited on a copper-grid-supported perforated transparent carbon coil.

2.5.3. *X-ray diffraction and particle size analysis*

The crystal structure of prepared nanoparticles was studied with an X-ray diffractometer (Siemens D5000, Germany) using Cu K_α radiation ($\lambda = 1.5418$ Å). The hydrodynamic sizes (d_H) and polydispersity were determined by dynamic light scattering technique. The instrument used was the Zetasizer Nanoseries ZEN 3600 (Malvern, UK). The measurements were carried out in triplicate and the average results are reported in this paper.

2.5.4. *Thermal gravimetry analysis*

Thermogravimetric analysis (TGA) experiments were performed using a TGA Q500 (TA Instruments, USA). Dried samples (10–20 mg) were placed in the TGA furnace and the measurements were carried out under nitrogen with a heating rate of 15 °C min^{-1} from 25 to 900 °C.

2.5.5. *Vibrating sample magnetometry*

The magnetization measurements were performed on a known amount of ferrofluid using a vibrating sample magnetometer (VSM; Nuovo Molspin, Newcastle-upon-Tyne, UK). The error on the magnetization measurement was 4%. The fitting of the Langevin function [eqn (1)] to the magnetometric profiles provides important information such as the crystal radius (r) and the specific magnetization (M_s) (37):

$$M = M_s L(x) \tag{1}$$

where $L(x) = \coth(x) - (1/x)$ is the Langevin function and $x = \boldsymbol{\mu} B_0 = k_B T$, with μ the magnetic moment of the particle, k_B the Boltzmann constant and T the absolute temperature.

2.5.6. *Nuclear magnetic relaxation dispersion profiles*

An additional way of determining the size is the measurement of the proton nuclear magnetic relaxation rate of water at different magnetic fields. Nuclear magnetic relaxation dispersion (NMRD) profiles were recorded with a fast field cycling relaxometer (Stelar, Mede, Italy) measuring the longitudinal relaxation rates (R_1) over a field range extending from 0.24 mT to 1 T. The temperature of the samples was adjusted to 37 °C with a precision of 0.1 °C. Additional longitudinal (R_1) and transverse (R_2) relaxation rate measurements at 0.47 and 1.41 T were obtained on Minispec Mq 20 and Mq 60 spin analyzers (Bruker, Karlsruhe, Germany).

For measuring the R_1 and R_2 relaxation rates at 7 T, T_1- and T_2-weighted phantom MRI images were acquired at different iron concentrations. The experiments were performed at room temperature on a 300 MHz (7 T) Bruker Biospec imaging system (Bruker, Ettlingen, Germany) equipped with a Pharmascan horizontal magnet. For T_1 measurements we used a rapid acquisition with relaxation enhancement (RARE)-T_1 map sequence (repetition time, TR, 117.6–15 000 ms; number of experiments, 6; echo time, TE, 14.5 ms; slice thickness, 1 mm; field of view, FOV, 3 cm; RARE factor, 2; matrix, 256 × 256; spatial resolution, 117 μm; total time scan, 40 min). T_2 was measured with a mutislice multiecho sequence (TR, 3000 ms; TE, 10.8 ms; number of echoes, 16; slice thickness, 1 mm; FOV, 4.42/4.47 cm; matrix, 256 × 256; spatial resolution, 173 μm × 175 μm; total scan time, 19 min).

The total iron concentration was determined by the measurement of the longitudinal relaxation rate R_1 according to the method previously described (36). Briefly, the samples were mineralized by microwave digestion (MLS-1200 Mega, Milestone, Analis, Namur, Belgium) and the R_1 value of the resulting solutions was recorded at 0.47 T and 37 °C, which allowed determination of the iron concentration, using eqn (2):

$$[\mathrm{Fe}] = \left(R_1{}^{\mathrm{sample}} - R_1{}^{\mathrm{diam}}\right) \times 0.0915 \tag{2}$$

where R_1^{diam} (s^{-1}) is the diamagnetic relaxation rate of water (0.36 s^{-1}) and 0.0915 ($s^{-1}\,mM^{-1}$) is the slope of the calibration curve.

The stability of the solution was studied by turbidimetry using a Turbiscan (Lab Expert Model, Formulaction, France).

2.6. *In vivo* MRI studies

The NMRI mice ($n = 3$) were anesthetized with 60 mg kg^{-1} body weight, i.p., of Nembutal (Sanofi, Brussels, Belgium). The experiments were performed on the previously mentioned 300 MHz (7 T) Bruker Biospec imaging system. The contrast agent was injected intravenously at a dose of 0.1 mmol iron kg^{-1} body weight. Images were acquired with RARE imaging protocol (TR = 3000 ms, effective echo time = 48.7 ms, RARE factor = 4, NEX = 4, matrix = 256 × 256, FOV = 5 cm × 5 cm, slice thickness 1 mm, 20 coronal slices, spatial resolution = 196 μm, TA = 12 min 48 s).

The signal intensity (SI) was measured in regions of interest drawn globally on the liver and the kidney, and in a region situated out of the image of the animal, representing the standard deviation of the noise (noise SD). The SI enhancement (ΔSNR%) was calculated according to eqn (3):

$$\Delta\ \mathrm{SNR\%} = \frac{\left(\mathrm{SI_{post}}/\mathrm{Noise\ SD}\right) - \left(\mathrm{SI_{pre}}/\mathrm{Noise\ SD}\right)}{\left(\mathrm{SI_{pre}}/\mathrm{Noise\ SD}\right)} \times 100 \tag{3}$$

where SI_{post} = post-contrast SI, and SI_{pre} = pre-contrast SI.

At the end of the MRI studies, the mice were sacrificed and the blood plasma and urine were collected for the measurement of iron concentration. The T_2 of blood plasma and urine was measured using a Bruker Minispec mq60 working at 60 MHz and 37 °C. The concentration of ultrasmall superparamagnetic iron oxide (USPIO) derivative was then calculated by relating the R_2^{Norm} (normalized by subtracting the R_2 of mice not injected with USPIO) of test samples to the transverse relaxivity, r_2, of USPIO derivative measured in blood plasma and urine.

3. RESULTS AND DISCUSSION

3.1. Preparation and characterization of PG-grafted Fe_3O_4 nanoparticles

The process for the synthesis of polyglycerol-grafted Fe_3O_4 nanoparticles is shown in Fig. 1. The Fe_3O_4 nanoparticles were synthesized by a chemical co-precipitation of Fe^{2+} and Fe^{3+} ions

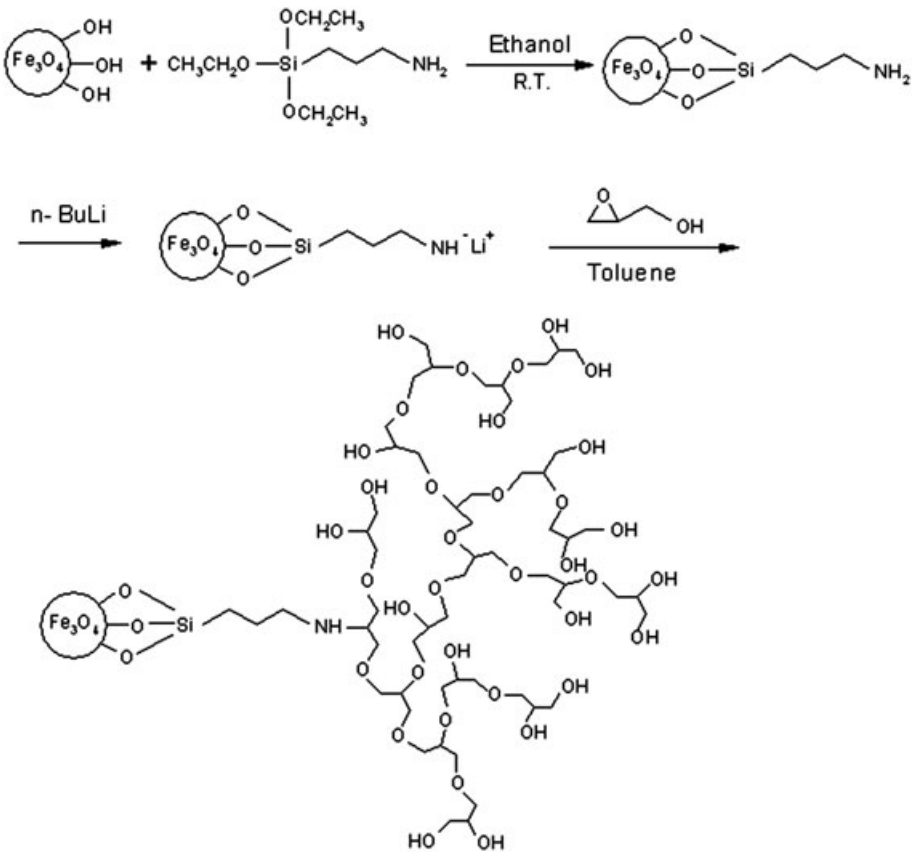

Figure 1. Surface modification of Fe_3O_4 nanoparticles with APTES, and anionic polymerization of glycidol on the surface.

under alkaline condition. The concentration ratio of Fe^{2+}/Fe^{3+} was 1:2, and the experiment was carried out under argon gas to prevent Fe^{2+} oxidation to Fe^{3+}. The Fe_3O_4 nanoparticles prepared by the co-precipitation method have several hydroxyl groups on the surface. APTES-modified MNPs were achieved by the silanization reaction between APTES and the hydroxyl groups on the surface of magnetite.

After deprotonation of APTES-modified nanoparticles with butyllithium, glycidol was polymerized on the surface of magnetite nanoparticles via *in-situ* anionic ring-opening polymerization (Fig. 1). As mentioned above, PG is completely water soluble and biocompatible, and hence, its grafting to magnetite nanoparticles induces excellent dispersibility of nanoparticles in water and results in water-based ferrofluids suitable for further bioapplications.

The chemical structure of Fe_3O_4 nanoparticles was characterized by FT-IR spectroscopy. Figure 2(a–c) shows the FT-IR spectra of pure Fe_3O_4, APTES-modified Fe_3O_4 and PG-grafted Fe_3O_4 nanoparticles, respectively. In IR spectra presented in Fig. 2, the absorption peak at 582 cm^{-1} belongs to the stretching vibration mode of Fe–O bonds in Fe_3O_4 nanoparticles. In the IR spectrum of APTES-modified Fe_3O_4 (Fig. 2b), the presence of Fe–O–Si bonds cannot be seen because it appears at around 584 cm^{-1} and therefore overlaps with the Fe–O vibration of magnetite nanoparticles. In comparison with bare Fe_3O_4 nanoparticles, APTES-modified Fe_3O_4 possesses absorption bands at 2854 and 2926 cm^{-1}, which belong to the symmetric and asymmetric stretching vibration of the CH_2 group. The absorption band at 1111 cm^{-1} is due to the stretching vibration of C–N bond, and the band at 1012 cm^{-1} belongs to the stretching vibration of the Si–O–Si bond. The formation of the Si–O–Si bond is attributed to silane groups undergoing a self-condensation reaction to form a polysiloxane film on the nanoparticle' surface (38).

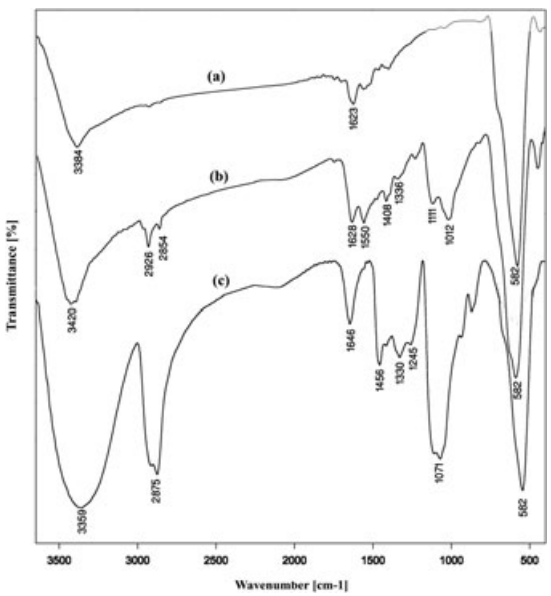

Figure 2. FT-IR spectra of (a) Fe_3O_4, (b) APTES-modified Fe_3O_4, and (c) PG-grafted Fe_3O_4.

Bands at 1336 and 1408 cm^{-1} correspond to the bending vibration of the CH_2 group. Furthermore, the two bands at 3420 and 1628 cm^{-1} can be ascribed to the N–H stretching and N–H bending vibrations, respectively (39). All of these bands indicate that the coupling agent APTES has been introduced onto the Fe_3O_4 MNPs surface.

Figure 2(c) shows the IR spectra of hyperbranched polyglycerol-grafted Fe_3O_4 nanoparticles. The broad band at 3359 cm^{-1} belongs to stretching vibration of the O–H bond. The broad and split peak at 2875 cm^{-1} is due to the strong overlapping of the C–H stretching (symmetric and asymmetric) of the polyglycerols tail. The bands at 1456, 1330 and 1245 cm^{-1} are attributed to the scissoring, wagging and twisting modes of bending vibration of the CH_2 group, respectively. The strong and broad band at 1071 cm^{-1} belongs to the CH_2–O bond.

Figure 3 shows an XRD pattern of Fe_3O_4 nanoparticles, which indicates a highly crystalline cubic spinel structure. The reflection peak positions and relative intensities of Fe_3O_4 nanoparticles agree well with the XRD pattern of magnetite in the literature (40), which confirms the structure of the magnetite.

The TEM micrographs of pure Fe_3O_4 nanoparticles (Fig. 4a) and PG-grafted nanoparticles (Fig. 4b) are shown in Fig. 4(a and b), respectively. The electron diffraction pattern (Fig. 4c), consisting of rings, indicates the good crystal structure of the Fe_3O_4 nanoparticles. It can be seen that the particles modified with hyperbranched polyglycerol are well dispersed, while the bare nanoparticles have a tendency to aggregate. This is a further confirmation of the encapsulation of Fe_3O_4 magnetic core by hyperbrached polyglycerol.

The surface-grafted magnetic nanoparticles could be easily dispersed in water to form a uniform suspension and be stably preserved for several months, suggesting that the aggregation tendency of particles is significantly weak, whereas the suspension made from the bare magnetic nanoparticles is completely precipitated from the solvent in only a few minutes without stirring. The stability measurement with turbiscan showed the high stability of PG-grafted nanoparticles. Figure 5 shows the PCS size distribution plot for PG-grafted nanoparticles, with a mean hydrodynamic size of about 39 nm.

The magnetite contents of APTES-modified magnetite and PG-grafted magnetite were measured through the TGA under nitrogen atmosphere condition at the heating rate of 15 °C min^{-1}. Figure 6 illustrates the TGA curves, depicting the variations of residual masses of the samples with temperature. The organic materials and magnetite of the samples were completely burned to generate gas products and converted into Fe_2O_3 at elevated temperatures, respectively. The magnetite amounts of samples can be estimated from the residual mass percentages. The absolute weight loss of the uncoated Fe_3O_4 was 5.4% (Fig. 6a) for the whole temperature range because of the removal of physically and chemically adsorbed water. Figure 6(b) shows the TGA curve

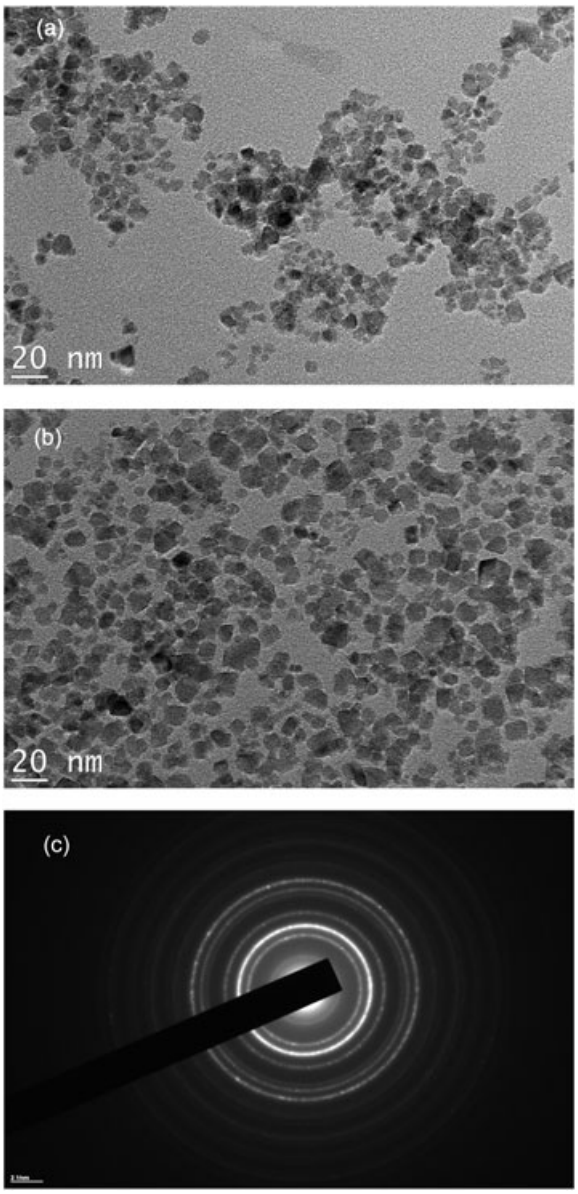

Figure 4. TEM images of (a) pure Fe_3O_4 nanoparticles; (b) PG-grafted Fe_3O_4 nanoparticles; and (c) electron diffraction pattern of pure Fe_3O_4 nanoparticles.

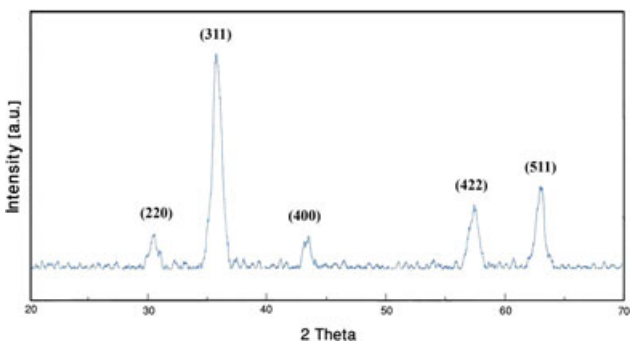

Figure 3. XRD pattern of Fe_3O_4 nanoparticles.

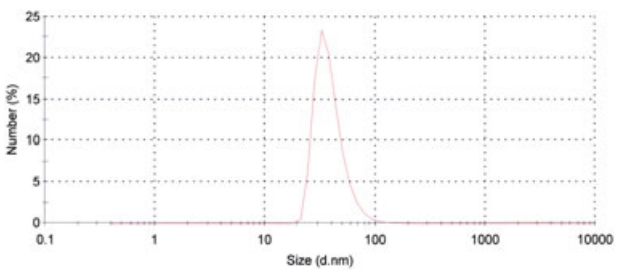

Figure 5. Size distribution plot of PG-grafted Fe_3O_4 nanoparticles.

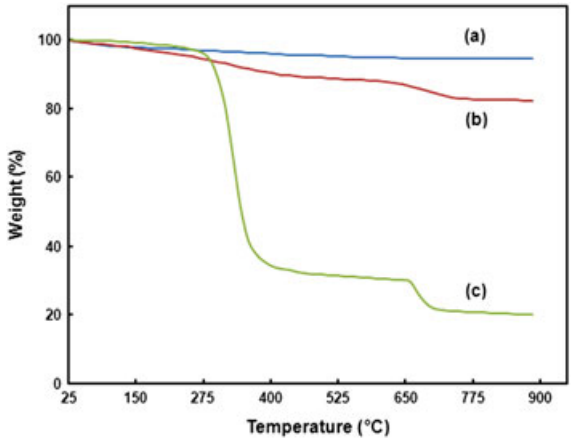

Figure 6. TGA curve of (a) pure Fe_3O_4, (b) APTES-modified, and (c) PG-grafted Fe_3O_4 nanoparticles.

of APTES-modified nanoparticles with a total weight loss of 17.7%. This weight loss happens in three steps: the first weight loss of 3.5% up to 200 °C can be attributed to evaporation of adsorbed water, and the aminosilane coating decomposition happens in two steps: 7.74% between 200 and 450 °C and 6.45% between 450 and 780 °C. Figure 6(c) shows that the decomposition for PG-grafted nanoparticles also happens in two steps. A large weight loss (68.72%) happens between 200 and 450 °C, which can be attributed to the decomposition of polyglycerol and also the organic part of APTES, and a second step happens at the same temperature of APTES-coated nanoparticles with the amount 11.26%. By considering these weight losses, the total amount of magnetite in PG-grafted nanoparticles is 20%.

3.2. Magnetometry and relaxometry

The magnetic properties of PG-grafted Fe_3O_4 nanoparticles were measured using VSM at room temperature. The hysteresis loop of PG-grafted Fe_3O_4 nanoparticles is shown in Fig. 7. As can be seen, it does not display magnetic remanence, and thus the nanoparticles are considered to be superparamagnetic. The M_s of PG-grafted Fe_3O_4 nanoparticles was about 46.6 emu g^{-1}, and the mean radius of nanoparticles obtained by this method was 5.9 nm.

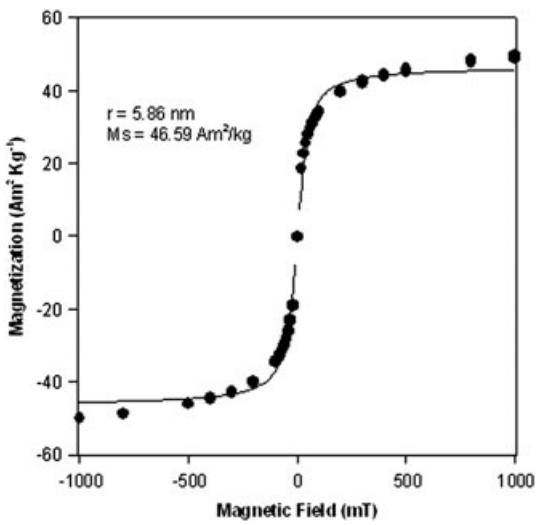

Figure 7. Hysterisis loop measured for PG-grafted Fe_3O_4 nanoparticles. The nanoparticles show superparamagnetic properties at room temperature and the M_s is about 46.6 emu g^{-1}.

The relaxation rates R_1 ($1/T_1$) and R_2 ($1/T_2$) were measured as a function of the iron molar concentration for the PG-grafted nanoparticles at 0.47, 1.41 and 7 T in order to calculate the r_1 and r_2 relaxivities (defined as the enhancement of the relaxation rate of water protons in 1 mmol l^{-1} solution of contrast agents). The relaxivities were calculated as the slope of relaxation rate versus iron concentration according to eqns (3) and (4), respectively (35):

$$R_1 = \frac{1}{T_1^{obs}} = r_1[Fe] + \frac{1}{T_1^{diam}} \quad (4)$$

$$R_2 = \frac{1}{T_2^{obs}} = r_2[Fe] + \frac{1}{T_2^{diam}} \quad (5)$$

where r_1 and r_2 are the longitudinal and transversal relaxivities, respectively, and T_1^{diam} and T_2^{diam} are the proton relaxation times in aqueous solutions without nanoparticles.

The r_1 and r_2 relaxivities, and r_2/r_1 ratio at different magnetic fields are summarized in Table 1. It is well known that the relaxivity ratio, r_2/r_1, is an important parameter to estimate the efficiency of T_2-contrast agents. In our work, the r_2/r_1 values were calculated to be 16.34 and 289.09 at 1.41, and 7 T, respectively, which is much larger than those of commercially available dextran-coated nanoparticles (Endorem; 11.9 at 1.5 T, and 82.7 at 7 T) (41), demonstrating that PG-grafted nanoparticles could perform well as T_2-contrast agents in magnetic resonance imaging. These higher values of r_2 relaxivities and thus r_2/r_1 ratio can be attributed to the higher hydrophilicity and also the branched structure of polyglycerol, which can induce better water retention around the magnetic core and hence enhance transverse relaxation induced by magnetic nanoparticles.

The nuclear magnetic relaxation dispersion profile of PG-grafted nanoparticles is shown in Fig. 8. Interpretation of the relaxation profiles (i.e. evaluation of the relaxivity as a function of the magnetic field) with appropriate theoretical models (42,43) provides information about the main properties of the superparamagnetic crystals, such as their specific magnetization (41.8 A m^2 kg^{-1}) and their radius ($r = 7.5$ nm). The corresponding value obtained by magnetometry (VSM) is $M_s = 46.6$ Am^2 kg^{-1} for magnetization and $r = 5.9$ nm for the crystal radius. As can be seen, the mean radius obtained by magnetometry is less than the amount obtained by relaxometry. This difference can be explained by distribution of crystal size, which influences the mean size obtained by various methods (44). The size dispersion is also responsible for the lower specific magnetization obtained

Table 1. *In vitro* relaxivity measurement of PG-grafted nanoparticles at 0.47 and 1.41 T (both at 37 °C) and 7 T (at room temperature)

Magnetic field (T)	r_1 (mM^{-1} s^{-1})	r_2 (mM^{-1} s^{-1})	r_2/r_1
0.47	26.2	158.3	6.04
1.41	8.77	143.3	16.34
7	0.623	180.1	289.09

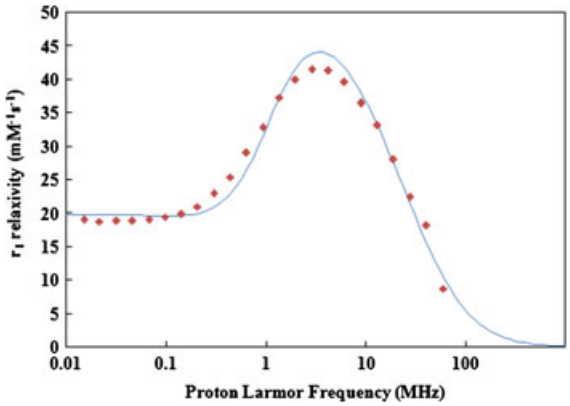

Figure 8. Nuclear magnetic relaxation dispersion profile of PG-grafted Fe_3O_4 nanoparticles at 37 °C.

by relaxometry compared with the amount obtained by magnetometry (45).

3.3. Phantom and *in vivo* MRI

Since superparamagnetic Fe_3O_4 nanoparticles are good T_2-type (negative) contrast agents in MRI, and PG is a biocompatible macromolecule, the effect of PG-grafted MNPs was investigated in terms of MR signal-enhancing property using a phantom test. Figure 9 shows T_2-weighted MR images of various concentrations of PG-grafted Fe_3O_4 nanoparticles in water. It can be seen that the MR signal intensity (related to the T_2 relaxation time in T_2-weighted images) for the samples of different concentrations is not identical. With increasing nanoparticle concentration in water, the MR signal is significantly decreased (negative contrast in T_2-weighted image). In the presence of an externally applied magnetic field, it is well known that superparamagnetic iron oxide nanoparticles create inhomogeneity in the magnetic field, affecting the microenvironment which results in dephasing of the magnetic moments of protons and hence T_2 shortening. The results indicate that the nanoparticles can generate high magnetic field gradients near the surface of the PG-grafted Fe_3O_4 nanoparticles.

The *in vivo* MRI studies were performed on NMRI mice. Figure 10 shows spin-echo abdomen images of a living mouse acquired before and after intravenous injection of the nanoparticles solution at different times. The injected dose was 100 μmol Fe kg^{-1} (~6 mg kg^{-1}) of body weight. We found a strong negative contrast in the liver and kidneys in T_2-weighted images 6 min after intravenous injection (Fig. 10).

It has been shown that commercial nanoparticles like Resovist applied through intravenous injection are rapidly recognized by the reticuloendothelial system and, therefore, are displaced from the blood compartment into the liver within 10 min (46). As can be seen from Fig. 10, our particles had a similar behavior within 6 min after injection. The negative contrast persisted for 80 min (in liver) to 110 min (in kidneys), but it weakened over time, suggesting that polyglycerol coating renders the nanoparticles stealth and possibly susceptible to renal excretion. The comparison of MRI images at different times after injection indicates that the kidneys are brightening over the time, the same as the renal pelvis and the ureter, although at this level the negative contrast persists. This phenomenon can be attributed to the high hydrophilicity and biocompatibility of polyglycerol, which facilitate the circulation of nanoparticles into the blood stream and limit their uptake by macrophages. These results are consistent with the studies of Wang *et al.* (33,47) and Weinhart *et al.* (48), who have pointed out that polyglycerol derivatives seem to be promising alternatives to polyethylene glycol owing to their furtivity, lack of cytotoxicity and high stability. Our PG-grafted Fe_3O_4 nanoparticles could thus be used as an MRI contrast agent for the diagnosis of liver and kidney lesions, avoiding the drawback of organ retention and the subsequent toxicity.

The ΔSNR% measured on RARE images of liver and kidneys (Fig. 11) confirmed the negative contrast produced by PG-grafted nanoparticles, which attained a maximum 84 min post-contrast for liver (−61%) and 6 min post-contrast for kidney (−56%). At the end of the imaging session, the negative contrast increased to −37% for kidney and to −40% in the case of liver.

The iron concentration was determined in blood plasma and urine at the end of the MRI studies, and we found 414 ± 72 μmol l^{-1} (29% of the injected dose) in blood plasma and 0.5 ± 0.4 μmol l^{-1} (0.035% of the injected dose) in urine, respectively. Therefore, since iron concentration in blood is

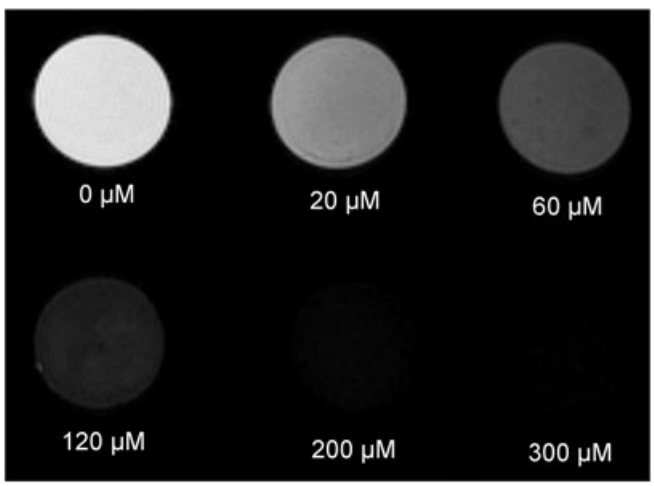

Figure 9. T_2-weighted MRI images (7 T, mutislice multiecho sequence: $TR = 4000$ ms, $TE = 80$ ms) of the PG-grafted Fe_3O_4 nanoparticles at various iron concentrations at room temperature.

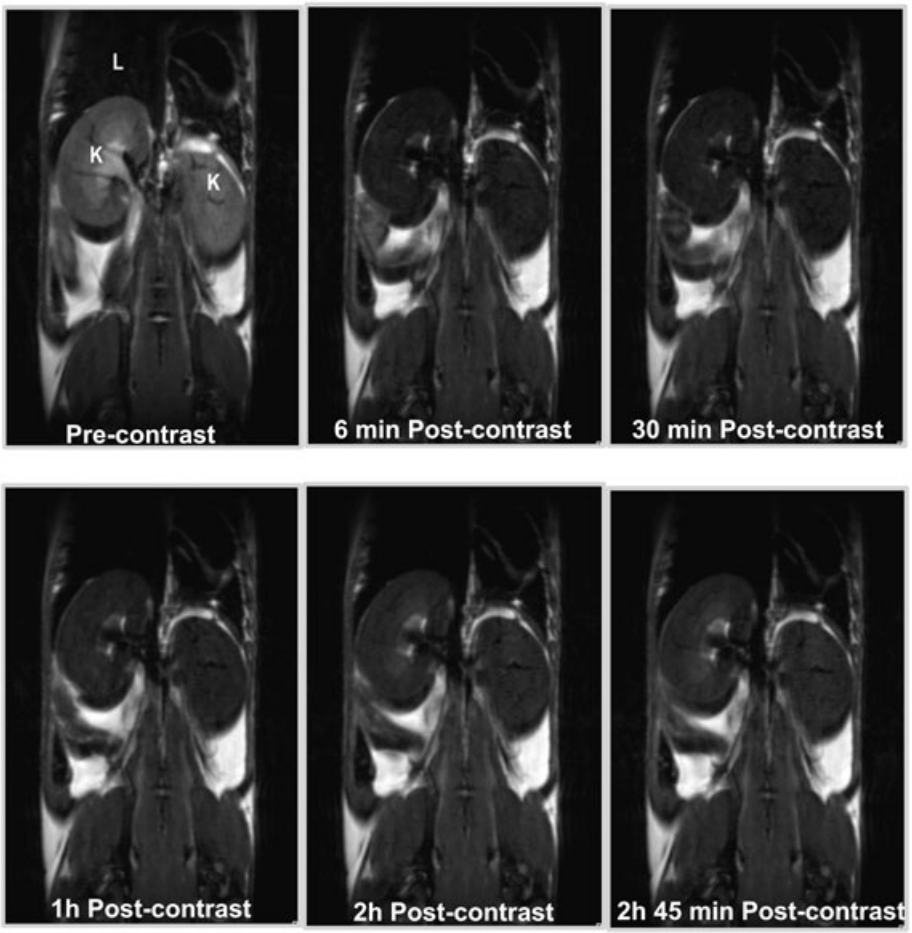

Figure 10. MRI images of a live mouse with a T_2-weighted spin-echo sequence (L, liver; K, kidney). Images were acquired before (pre-contrast) and 6 min, 30 min, 1 h, 2 h and 2 h 45 min after intravenous injection of PG-grafted nanoparticles.

decreased in the absence of a major liver uptake, it is possible that renal excretion occurs. The urine concentration was low almost 3 h after administration, but it is premature to draw a final conclusion in the absence of a kinetics study of the renal excretion. Future experiments will help to elucidate the excretion mechanism of this particular compound.

4. CONCLUSION

We prepared a highly stable ferrofluid by chemical surface modification of superparamagnetic iron oxide nanoparticles. With this aim, after surface modification of magnetite nanoparticles with 3-aminopropyltriethoxysilane, polyglycerol was grafted through ring-opening anionic polymerization. The surface-modified nanoparticles exhibited long-term colloidal stability. Since polyglycerol is a water-soluble and biocompatible polymer with lots of hydroxyl groups on the periphery, it can be considered as a highly potential platform for further vectorization to target different organs and diseases in molecular imaging. The obtained results show their greater potential as negative MRI contrast agents in comparison with commercially available compounds. The PG-grafted ferrofluid was injected intravenously in mice and studied by MRI. Nanoparticles accumulated rapidly in liver and also in kidneys within the first 6 min after administration, but they were washed out about 80 min (in liver) to 110 min (in kidneys) post-injection, conceivably owing to the hydrophilic and stealth coating of these nanoparticles.

Acknowledgments

The authors sincerely acknowledge Sarah Belaid (NMR and Molecular Imaging Laboratory, University of Mons, Belgium) for her help in acquiring and analyzing the TGA data. Fruitful discussions with Professors Ali akbar Entezami (Faculty of Chemistry, University of Tabriz, Iran) and Mahmoud Nazarpoor (Faculty of Paramedicine, Tabriz University of Medical Sciences, Iran) are gratefully acknowledged. The Laboratory of Polymeric and Composite Materials (Professor Ph. Dubois) and the Biological Physics Department (Professor P. Gillis) of the University of Mons are thanked for access to their TGA and magnetometer equipment. The financial support of the University of Tabriz and Iranian Nanotechnology Society are kindly acknowledged. This work was also partially supported by the Fonds de la Recherche Scientifique, the ARC Program 05/10-335 of the French Community of Belgium and the ENCITE program of the European Community. The support and sponsorship organized by COST Action D38 'Metal-based Systems for Molecular Imaging Applications' and the EMIL program are kindly acknowledged.

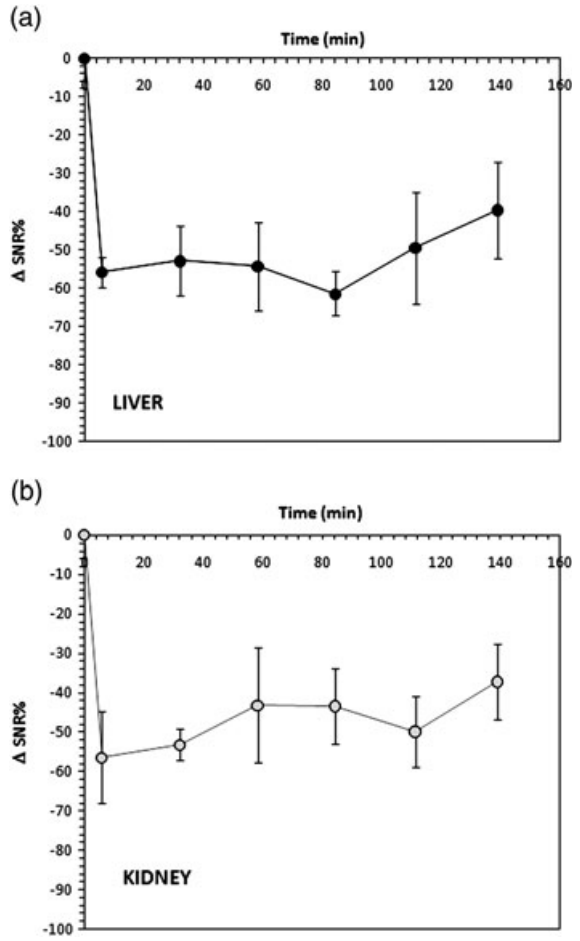

Figure 11. Calculated ΔSNR% for (a) liver and (b) kidney over the time after intravenous injection of PG-grafted nanoparticles.

REFERENCES

1. Rinck PA. Magnetic Resonance in Medicine. Wiley Blackwell: Berlin, 2003.
2. Yallapu MM, Othman SF, Curtis ET, Gupta BK, Jaggi M, Chauhan SC. Multi-functional magnetic nanoparticles for magnetic resonance imaging and cancer therapy. Biomaterials 2011; 32: 1890–1905.
3. Terreno E, Castelli DD, Viale A, Aime S. Challenges for molecular magnetic resonance imaging. Chem Rev 2010; 110: 3019–3042.
4. Laurent S, Forge D, Port M, Roch A, Robic C, Vander Elst L, Muller RN. Magnetic iron oxide nanoparticles: synthesis, stabilization, vectorization, physicochemical characterizations, and biological applications. Chem Rev 2008; 108: 2064–2110.
5. Bulte JW, Hoekstra Y, Kamman RL, Magin RL, Webb AG, Briggs RW, Go KG, Hulstaert CE, Miltenyi S, The TH, Deleij L. Specific MR imaging of human lymphocytes by monoclonal antibody-guided dextran–magnetite particles. Magn Reson Med 1992; 25: 148–157.
6. Fattahi H, Laurent S, Liu F, Arsalani N, Vander Elst L, Muller RN. Magnetoliposomes as multimodal contrast agents for molecular imaging and cancer nanotheragnostics. Nanomedicine 2011; 6(3): 529–544.
7. Cormode DP, Jarzyna PA, Mulder WJM, Fayad ZA. Modified natural nanoparticles as contrast agents for medical imaging. Adv Drug Deliv Rev 2010; 62: 329–338.
8. Laurent S, Boutry S, Mahieu I, Vander Elst L, Muller RN. Iron oxide based MR contrast agents: from chemistry to cell labeling. Curr Med Chem 2009; 16: 4712–4727.
9. Sun C, Du K, Fang C, Bhattarai N, Veiseh O, Kievit F, Stephen Z, Lee D, Ellenbogen RG, Ratner B, Zhang M. PEG-mediated synthesis of highly dispersive multifunctional superparamagnetic nanoparticles: their physicochemical properties and function in vivo. ACS Nano 2010; 4: 2402–2410.
10. Liu F, Laurent S, Fattahi H, Vander Elst L, Muller RN. Superparamagnetic nanosystems based on iron oxide nanoparticles for biomedical imaging. Nanomedicine 2011; 6(3): 519–528.
11. Fan C, Gao W, Chen Z, Fan H, Li M, Deng F, Chen Z. Tumor selectivity of stealth multi-functionalized superparamagnetic iron oxide nanoparticles. Int J Pharm 2011; 404: 180–190.
12. Abdalla MO, Karna P, Sajja HK, Mao H, Yates C, Turner T, Aneja R. Enhanced noscapine delivery using uPAR-targeted optical-MR imaging trackable nanoparticles for prostate cancer therapy. J Control Release 2011; 149: 314–322.
13. Renard P-E, Lortz R, Senatore C, Rapin J-P, Buchegger F, Petri-Fink A, Hofmann H, Doelker E, Jordan O. Magnetic and in vitro heating properties of implants formed in situ from injectable formulations and containing superparamagnetic iron oxide nanoparticles (SPIONs) embedded in silicamicro particles for magnetically induced local hyperthermia. J Magn Magn Mater 2011; 323: 1054–1063.
14. Chen F, Shi R, Xue Y, Chen L, Wan Q-H. Templated synthesis of monodisperse mesoporous maghemite/silica microspheres for magnetic separation of genomic DNA. J Magn Magn Mater 2010; 322: 2439–2445.
15. Burtea C, Laurent S, Mahieu I, Larbanoix L, Roch A, Port M, Rousseaux O, Ballet S, Murariu O, Toubeau G, Corot C, Vander Elst L, Muller RN. In vitro biomedical applications of functionalized iron oxide nanoparticles, including those not related to magnetic properties. Contrast Media Mol Imag 2011; 6(4): 236–250.
16. Weissleder R, Bogdanov A, Neuwelt EA, Papisov M. Long-circulating iron oxides for MR imaging. Adv Drug Deliv Rev 1995; 16: 321–334.
17. Kaim AH, Wischer T, Reilly T, Jundt G, Frohlich J, Schulthess GK, Allegrini PR. MR imaging with ultrasmall superparamagnetic iron oxide particles in experimental soft-tissue infections in rats. Radiology 2002; 225: 808–814.
18. Lacava LM, Lacava ZG, Silva MF, Silva O, Chaves SB, Azevedo RB, Pelegrini F, Gansau C, Buske N, Sabolovic D, Morais PC. Magnetic resonance of a dextran-coated magnetic fluid intravenously administered in mice. Biophys J 2001; 80: 2483–2486.
19. Lin H, Watanabe Y, Kimura M, Hanabusa K, Shirai H. Preparation of magnetic poly(vinyl alcohol) (PVA) materials by in situ synthesis of magnetite in a PVA matrix. J Appl Polym Sci 2003; 87: 1239–1247.
20. Lee SJ, Jeong JR, Shin SC, Kim JC, Chang YH, Lee KH, Kim JD. Magnetic enhancement of iron oxide nanoparticles encapsulated with poly(D,L-latide-co-glycolide). Colloids Surf A 2005;255:19–25.
21. Kohler N, Sun C, Fichtenholtz A, Gunn J, Fang C, Zhang MQ. Methotrexate-immobilized poly(ethylene glycol) magnetic nanoparticles for MR imaging and drug delivery. Small 2006; 2: 785–792.
22. Liu HL, Ko SP, Wu JH, Jung MH, Min JH, Lee JH, An BH, Kim YK. One-pot polyol synthesis of monosize PVP-coated sub-5 nm Fe_3O_4 nanoparticles for biomedical applications. J Magn Magn Mater 2007; 310: 815–817.
23. Arsalani N, Fattahi H, Nazarpoor M. Synthesis and characterization of PVP-functionalized superparamagnetic Fe_3O_4 nanoparticles as an MRI contrast agent. eXPRESS Polym Lett 2010; 4: 329–338.
24. Lee H, Lee E, Kim DK, Jang NK, Jeong YY, Jon S. Antibiofouling polymer-coated superparamagnetic iron oxide nanoparticles as potential magnetic resonance contrast agents for in vivo cancer imaging. J Am Chem Soc 2006; 128: 7383–7389.
25. Feng B, Hong RY, Wang LS, Guo L, Li HZ, Ding J, Zheng Y, Wei DG. Synthesis of Fe_3O_4/APTES/PEG diacid functionalized magnetic nanoparticles for MR imaging. Colloid Surf A 2008; 328: 52–59.
26. Barrera C, Herrera AP, Rinaldi C. Colloidal dispersions of monodisperse magnetite nanoparticles modified with poly(ethylene glycol). J Colloid Interf Sci 2009; 329: 107–113.
27. Cao H, He J, Deng L, Gao X. Fabrication of cyclodextrin-functionalized superparamagnetic Fe_3O_4/amino-silane core shell nanoparticles via layer-by-layer method. Appl Surf Sci 2009; 225: 7974–7980.
28. Kautz H, Sunder A, Frey H. Control of the molecular weight of hyperbranched polyglycerols. Macromol Symp 2001; 163: 67–73.
29. Liu Z, Janzen J, Brooks DE. Adsorption of amphiphilic hyperbranched polyglycerol derivatives onto human red blood cells. Biomaterials 2010; 31(12): 3364–3373.
30. Calderon M, Graeser R, Kratz F, Haag R. Development of enzymatically cleavable prodrugs derived from dendritic polyglycerol. Bioorg Med Chem Lett 2009; 19: 3725–3728.
31. Calderon M, Warnecke A, Graser R, Haag R, Kratz F. Development of enzymatically cleavable doxorubicin conjugates with polyglycerol. J Control Release 2008; 132: e54–e55.

32. Gottschalk C, Wolf F, Frey H. Multi-arm star poly (L-lactide) with hyperbranched polyglycerol core. Macromol Chem Phys 2007; 208: 1657–1665.
33. Wang L, Neoh KG, Kang ET, Shuter B, Wang S-C. Superparamagnetic hyperbranched polyglycerol-grafted Fe_3O_4 nanoparticles as novel magnetic resonance imaging contrast agent: an in vitro assessment. Adv Func Mater 2009; 19: 2615–2622.
34. Massart R, Cabuil V. Effect of some parameters on the formation of colloidal magnetite in alkaline medium: yield and particle size control. J Chem Phys 1987; 84: 967–973.
35. Burtea C, Laurent S, Vander Elst L, Muller RN. Contrast agents: magnetic resonance. Handb Exp Pharmacol 2008; 185: 135–165.
36. Ozmen M, Can K, Arslan G, Tor A, Cengeloglu Y, Ersoz M. Adsorption of Cu(II) from aqueous solution by using modified Fe_3O_4 magnetic nanoparticles. Desalination 2010; 254: 162–169.
37. Forge D, Gossuin Y, Roch A, Laurent S, Vander Elst L, Muller RN. Development of magnetic chromatography to sort polydisperse nanoparticles in ferrofluids. Contrast Media Mol Imag 2010; 5: 126–132.
38. Flesch C, Delaite C, Dumas P, Bourgeat-Lami E, Duguet E. Grafting of poly(ε-caprolactone) onto maghemite nanoparticles. J Polym Sci Pol Chem 2004; 42: 6011–6020.
39. Heiney PA, Gruneberg K, Fang J, Dulcey C, Shashidhar R. Structure and growth of chromophore-functionalized (3-aminopropyl) triethoxysilane self-assembled on silicon. Langmuir 2000; 16: 2651–2657.
40. Abdel-Hameed SAM, Hessien MM, Azooz MA. Preparation and characterization of some ferromagnetic glass–ceramics contains high quantity of magnetite. Ceram Int 2009; 35: 1539–1544.
41. Basly B, Felder-Flesch D, Perriat P, Billotey C, Taleb J, Pourroy G, Begin-Colin S. Dendronized iron oxide nanoparticles as contrast agents for MRI. Chem Commun 2010; 46: 985–987.
42. Roch A, Muller RN, Gillis P. Theory of proton relaxation induced by superparamagnetic particles. J Chem Phys 1999; 110: 5403–5411.
43. Roch A, Gillis P, Ouakssim A, Muller RN. Proton relaxation in superparamagnetic aqueous colloids: a new tool for the investigation of ferrite crystal anisotropy. J Magn Magn Mater 1999; 201: 77–79.
44. Ouakssim A, Fastrez S, Roch A, Laurent S, Gossuin Y, Pierart C, Vander Elst L, Muller RN. Control of the synthesis of magnetic fluids by relaxometry and magnetometry. J Magn Magn Mater 2004; 1711: 272–276.
45. Radermacher KA, Beghein N, Boutry S, Laurent S, Vander Elst L, Muller RN, Jordan BF, Gallez B. In vivo detection of inflammation using pegylated iron oxide particles targeted at E-selectin. Invest Radiol 2009; 44: 398–404.
46. Thunemann AF, Schutt D, Kaufner L, Pison U, Mohwald H. Maghemite nanoparticles protectively coated with poly(ethylene imine) and poly(ethylene oxide)-block-poly(glutamic acid). Langmuir 2006; 22: 2351–2357.
47. Wang L, Noeh KG, Kang E-T, Shuter B. Multifunctional polyglycerol-grafted Fe_3O_4@SiO_2 nanoparticles for targeting ovarian cancer cells. Biomaterials 2011; 32: 2166–2173.
48. Weinhart M, Grunwald I, Wyszogrodzka M, Gaetjen L, Hartwig A, Haag R. Linear poly(methyl glycerol) and linear polyglycerol as potent protein and cell resistant alternatives to poly(ethylene glycol). Chem Asian J 2010; 5(9): 1992–2000.